Journal Pre-proof

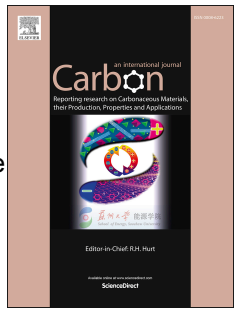

New insights into oxygen surface coverage and the resulting two-component structure of graphene oxide

Ignacio Martin-Gullon, Juana M. Pérez, Daniel Domene, Anibal J.A. Salgado-Casanova, Ljubisa R. Radovic

PII: S0008-6223(19)31127-3

DOI: https://doi.org/10.1016/j.carbon.2019.11.003

Reference: CARBON 14760

To appear in: *Carbon*

Received Date: 26 September 2019

Revised Date: 1 November 2019

Accepted Date: 2 November 2019

Please cite this article as: I. Martin-Gullon, J.M. Pérez, D. Domene, A.J.A. Salgado-Casanova, L.R. Radovic, New insights into oxygen surface coverage and the resulting two-component structure of graphene oxide, *Carbon* (2019), doi: https://doi.org/10.1016/j.carbon.2019.11.003.

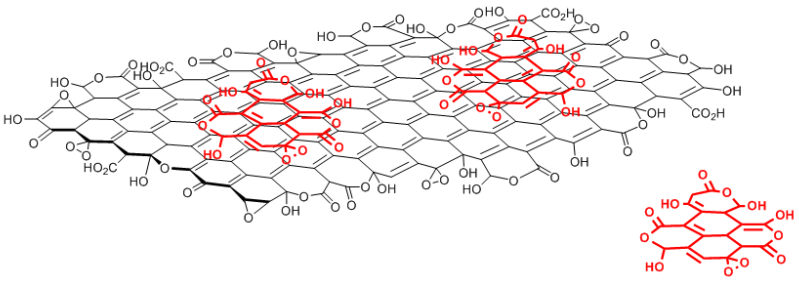

New insights into oxygen surface coverage and the resulting two-component structure of graphene oxide

Ignacio Martin-Gullon[1*], Juana M. Pérez[1], Daniel Domene[1], Anibal J.A. Salgado-Casanova[2], Ljubisa R. Radovic[2,3]*

[1]Chemical Engineering Department, University of Alicante, Alicante 03690, Spain

[2]Department of Chemical Engineering, University of Concepción, Chile

[3]Department of Energy and Mineral Engineering, The Pennsylvania State University, University Park, PA 16802, USA.

Abstract

Elucidating the essential details of the structure of graphene oxide (GO) is still a challenge. There is no consensus in the increasingly abundant literature, especially relating to the epoxy groups as the main surface complexes in the basal plane, as well as the simultaneous presence of GO sheets and oxidative debris (OD), with a large difference in their oxygen content. In the present work we characterized the base-washed GO (bwGO) sheets, the OD and the humic fraction of the OD obtained by base digestion, when the parent GO was dispersed by applying sonication, a routine procedure when starting from dried graphite oxide. When sonication is not applied, the amount of OD detected is considerably lower, indicative of its formation before base digestion. The presence of lactols and carboxylic anhydrides as the dominant surface complexes at graphene edges is consistent with all the characterization results, as well as with the general knowledge of surface chemistry of carbon materials ranging from coal to graphite. These findings suggest that the Hummers-Offeman reaction produces a chemical scissor effect during the water/hydrogen peroxide quenching step, yielding a broad size distribution of GO sheets, with little in-plane oxidation and the vast majority of edges being oxidized to form oxepinone-type functionalities.

* Corresponding authors. Email gullon@ua.es (I. Martin-Gullon) and lrr3@psu.edu (L.R. Radovic)

1. Introduction

Graphene oxide (GO) could be described as a two-dimensional material derived from graphene when oxygen surface functionalities are introduced both at the edges and within the basal plane to yield an oxygen-decorated graphene sheet [1]. The most common approach to prepare GO is the modified Hummers-Offeman methodology [2,3]; the three steps of this methodology were identified by Dimiev and Tour [4]. In the first step the conversion of graphite to the sulfuric acid-graphite intercalation compound takes place. Secondly, diffusion of the oxidizing agent, $KMnO_4$, into thus preformed galleries yields the pristine graphite oxide (pGO). The dimanganse heptoxide (Mn_2O_7), formed in highly concentrated H_2SO_4, is presumably responsible for oxidizing graphite on both the edges and the basal planes [1], as well as for the formation of organosulfates [5]. In the final step, the mixture is treated with excess water, which results in a loss of graphite interlayer registry, with the hydrolysis of some covalent organosulphates and, according to Kang *et al.*[6], in additional oxidation of pGO by the permanganate ions. Subsequent addition of hydrogen peroxide solubilizes all the manganese to Mn^{2+}, allowing its separation from the solid graphite-derived phase, yielding GO layers that can be exfoliated easily and separated individually by sonication [7]; excess of H_2O_2 presumably affects the resultant GO to some extent [8]. Graphite oxide (stacked sheets) and its derivative GO (single layer) are terms that are indistinctly used too often, even sometimes are both denoted as GO in the same study [9]; this can create misunderstandings, especially regarding the number of stacked layers. However, in the evidence of evidence to the contrary, the chemical composition of both graphite oxide and GO is considered equivalent [1].

Over the past decades, different models for the structure of GO have been proposed. The early ones envisioned a homogenenously oxidized structure [10,11] which turned out not to be consistent with detailed characterization studies. The Lerf-Klinowski model [12] is the most cited one; indeed, it served as the basis for subsequent models, adopted to explain both GO and reduced GO (rGO) structures [13]. It envisions a non-stoichiometric structure containing intercalated water between the layers and the GO with two distinct regions [12]: (i) isolated unoxidized aromatic domains and (ii) aliphatic six-membered rings, bonded to oxygen functionalities, single-bond epoxides and tertiary alcohols on the basal plane

(responsible for producing a flat layered structure), and carboxylic groups located at the edges of these layers. The use of ^{13}C-NMR has been essential for postulating the epoxide prevalence among the basal-plane surface functionalities, based on the very early assumption of Hofmann and Holst [1], favored over ether bridges proposed by Mermoux *et al.* [14] using the same technique. Their presence can explain the insulating nature of the material as a consequence of the isolated aromatic domains, whose conductivity could be restored through a reduction treatment [15–17]. Gao *et al.* [18] complemented this model by indicating the common presence at the edges of five- and six-membered ring lactols (with additional lactone groups in the same cyclic structures), detected also by ^{13}C-NMR. Dimiev *et al.* [19] also detected such structural features by ^{13}C-NMR and argued that they are mainly formed at vacancies rather than at edges, as a result of hydrolysis of organosulfates in excess water.

A new way to explain the more complex structure of GO was first proposed by Rourke *et al.* [20]: two distinct non-covalently complexed components, with a large difference in their oxygen content, which can be separated by a base wash. The majority component is insoluble and is composed of large and slightly oxidized graphene-like sheets (bwGO). The much less abundant and much more oxidized soluble fragments - oxidative debris (OD) - strongly adhere to these flat bwGO entities and are composed of polyaromatic molecules of widely varying sizes and with a large number of oxygen functionalities anchored to the edges. In fact, the early literature, before the seminal work of Hummers and Offeman [21], already indicated that aqueous $KMnO_4$ treatments of coals and cokes produced aromatic polycarboxylic acids [22,23]; the same acids (including mellitic acid) were obtained when graphite oxide is produced using chlorate-based oxidation methods [24], as corroborated recently by Lerf [25]. Consequently, OD acts as a surfactant able to disperse clean bwGO sheets. This assumption was based on results previously obtained using carbon nanotubes [26–28] or carbon fibers [29]. Because OD is rich in oxygen groups, it is responsible for most of the cumulative UV-Vis and IR absorption, as well as the photoluminescence of G-O, whereas bwGO contains fewer oxygen groups and hardly contributes to the previously mentioned properties [30]. Since OD was separated from bwGO by the different water solubility at alkaline pH, a further classification can be done by analogy with organic

matter components in soils [31] (*humus*): bwGO is equivalent to *humin* (insoluble at any pH) and OD (soluble at alkaline pH) is composed of humic-like fragments (equivalent to *humic acids*, insoluble at acidic pH) and fulvic-like substances (equivalent to *fulvic acids*, soluble at any pH), the main difference being the higher molecular weight of the former with respect to the latter.

Rodríguez-Pastor *et al*. [31] proposed a mechanistic GO formation model based on such dual structure, where $KMnO_4$ oxidation takes place in the intercalated layers during the GO formation and effects "scissor-like" cutting of the basal plane, thus yielding oxygen groups mainly at graphene edges, and resulting in randomly distributed sheets of widely varying sizes, from molecular species with very high oxygen-to-carbon (O/C) ratio to μm-size sheets with much lower O/C ratio. From TEM images, the formation of such OD was corroborated, as evidenced by a large variety of dots on the surface of G-O whose presence had not been given the importance that it deserves [32]. Although this two-component model is now widely accepted, it also generated some controversy. Thus, for example, Dimiev and Polson [33] proposed an alternative explanation by suggesting that OD formation occurs during the base wash treatment, by virtue of consecutive OH^- attack which eventually causes C-C bond cleavage and thus generates OD during the base digestion. Naumov *et al.* [34] also questioned the two-component model in a study of fluorescence properties of GO and bwGO of different oxidation levels. It is important to recall that the Hummers conditions (acid medium and large excess of $KMnO_4$) produce a total excision of double bonds, as corroborated by the group of Tour [35] using carbon nanotubes to form GO nanoribbons without applying any base wash treatment (TEM and AFM images showed evidence of OD), where the CNT uzipping is an intercalation-driven process [36]. Furthermore, Liscio *et al.* [37] demonstrated that sonication fragments the 2D sheets and could thus promote OD formation. Indeed, sonication treatments were used before a general procedure was adopted for identifying and quantifying the bwGO and OD [20,33]. There is no doubt that the essential details of the structure of GO remain a challenging topic and a satisfactory structural and compositional model has yet to emerge, as evidenced by the continuous influx of recent studies [8,38–40].

In the present study, GO was first synthesized using the Hummers-Offeman procedure. Our subsequent purpose is to verify whether OD formation takes place during the Hummers-Offeman reaction or during the base wash treatment. Detailed characterization of the different components provides a deeper understanding of GO structure, which is essential for its optimal applicability; indeed, a more detailed knowledge of this surface chemistry is recognized as being critical in a wide range of emerging applications, including biomedicine, multi-functional composites, catalysis and energy storage. Specifically, two different base digestion treatments, NaOH [20] and NH_3 [41], were applied to two different GO samples: dried graphene oxide (dGO), which was redispersed by applying sonication before base digestion (as regularly reported in the literature, e.g. Rourke *et al.* [20] and Dimiev and Polson [33]), and a non-dried and wet sample directly from the filter cake of GO production (cGO), which does not require sonication for dispersion prior to the base digestion step. In all cases, bwGO and OD were isolated and characterized from the base digestion step. In particular, X-ray photoelectron spectroscopy (XPS), thermogravimetry coupled with mass spectrometry (TG-MS), transmission electron microscopy (TEM), X-ray diffraction (XRD) and Fourier-transform infrared spectroscopy (FT-IR) were used in an attempt to elucidate the mechanism of formation of the two components of GO.

2. Methodology

2.1. Materials

Natural expanded graphite BNB90 was supplied by Timcal (Bodio, Switzerland). This material exhibits an average flake thickness of 35 nm and flake dimensions of 50 μm. $KMnO_4$, $NaNO_3$, H_2SO_4 (95%), HCl (37%) and NH_3 (30%) were supplied by VWR. H_2O_2 (33 vol%) and NaOH were purchased from Fisher.

2.2. Preparation of dGO and cGO

Some 5 g of graphite, 350 mL of H_2SO_4 and 5 g of $NaNO_3$ were mixed and stirred at room temperature. After 3 h, 20 g of $KMnO_4$ were slowly added and the suspension was stirred for 2 h. Subsequently, the temperature was increased to 55 ºC and kept for 1 h, forming the

pristine graphite oxide (pGO). Once the reaction was complete, the mixture was heated to 70 ºC and then immediately cooled to room temperatures and poured into a 500-mL flask containing ice/cold water with 40 mL of H_2O_2 (33 vol%); this prevents MnO_2 precipitation and produces graphite oxide. After filtration, the solid cake was washed with 50 mL of HCl (20 vol%) for 30 min with stirring and repeated filtering. Finally, washing and filtration was repeated with H_2O (100 mL), yielding a wet-cake graphite oxide (cGO) when all the liquid had passed through the filter. A drying treatment in an oven at 70 ºC overnight yields a dried-cake graphite oxide (dGO). The water content of cGO is thus determined. A schematic diagram of the sample preparation procedure is available in the Supplementary Data. In an ancillary experiment, a specific GO sample (eGO) was synthetized following Hummers-Offeman methodology modified by Eigler *et al.* [42], in order to keep the temperature below 10 ºC during both the oxidation step and the water addition step.

2.3. Isolation of OD

2.3.1. Treatment with NaOH

Some 1.5 g of dGO was suspended in 800 mL of H_2O by bath sonication for 20 min, forming exfoliated dGO. When the procedure is performed starting from cGO, the same amount of GO (including its moisture content) was suspended in 800 mL H_2O by simple mixture stirring, yielding spontaneously and instantly a stable and homogeneous suspension of exfoliated cGO. The following NaOH digestion was performed with each sample: 6.75 g of NaOH pellets were slowly added to the suspension with stirring, increasing the pH to ~13 and the temperature to 70 ºC over 1 hour. After cooling to room temperature, the mixture was centrifuged at 14000 rpm for 30 min, yielding a precipitated black solid that contains the bwGO and a slightly brownish clear supernatant that contains the oxidative debris (OD-dGO_{NaOH} or OD-cGO_{NaOH}). The bwGO samples were re-suspended in 300 mL of H_2O and neutralized with HCl (20 vol%). The mixture was then stirred at 70 ºC for 1 h; after cooling, three more water washing/centrifugation steps followed, obtaining a black solid after oven-drying at 70 ºC (bw-dGO_{NaOH} or bw-cGO_{NaOH}). The supernatant containing OD was reprotonated at pH 2 by adding HCl (20 vol%), which resulted in a pale yellow solution and a solid precipitate. These two fractions were separated by centrifugation at

14000 rpm for 30 min. The pale yellow solution contains the fulvic-like molecules suspended in water (fl-dGO$_{NaOH}$ or fl-cGO$_{NaOH}$), and the precipitated solid corresponds to humic-like fragments (hu-dGO$_{NaOH}$ or hu-cGO$_{NaOH}$). The bwGO and hu-GO weight fractions were determined gravimetrically.

2.3.2 Treatment with NH_3

The 800-mL suspensions for dGO and cGO were prepared according to the procedure described in section 2.3.1. Subsequently, 30 mL of concentrated NH_4OH were slowly added to the suspension with stirring yielding pH ~13, and the mixture was then digested at 70 ºC for 1 h. After cooling to room temperature, the suspension was centrifuged at 14000 rpm for 30 min; two fractions were obtained, a black solid that contains the base-washed graphene oxide (bw-dGO$_{NH3}$ or bw-cGO$_{NH3}$) and a supernatant that contains the OD (OD-dGO$_{NH3}$ or OD-cGO$_{NH3}$). The bwGO samples were reprotonated and water-washed following the same procedure described in the previous section. On the other hand, a measured portion of the supernatant was simply vacuum-evaporated (including excess ammonia) in a rotovapor, yielding dried OD (OD-dGO$_{NH3}$ or OD-cGO$_{NH3}$), which was gravimetrically quantified. Another weighted portion of the supernatant was then reprotonated to pH 2 by adding HCl (20 vol%), resulting in a colorless solution and a solid precipitate. These two fractions were separated by centrifugation at 14000 rpm for 30 min. The colorless solution contains the fulvic-like molecules (fl-dGO$_{NH3}$ or fl-cGO$_{NH3}$) suspended in water; the solid corresponds to humic-like fragments (hu-dGO$_{NH3}$ or hu-cGO$_{NH3}$), and it was quantified gravimetrically. Consequently, base-wash graphene oxide, humic fraction and fulvic fraction (by difference with OD) were all quantified in the ammonia treatment. A schematic diagram of the sample preparation procedure is included in the Supplementary Data.

2.4. Characterization

X-ray photoelectron spectroscopy (XPS) was carried out with a K-alpha spectrometer (Thermo-Scientific); the surface atomic O/C ratio was calculated by the integration of survey spectra, and analysis of functional groups bonded to C was performed by

deconvoluting the C_{1s} spectra. Two different spectra in different zones of the sample were acquired, and their reproducibility was good. Thermogravimetric and mass spectrometry analysis (TG-MS) was performed using a Mettler Toledo apparatus (TGA/SDT851e/LF/1600 coupled with a Thermostat GSD301T) in order to measure the weight loss and gas evolution upon thermal decomposition of samples of GO, bwGO, and OD-like materials; these experiments were carried out under He atmosphere, from room temperature to 1000 ºC at 10 ºC/min, with m/z = 18 (H_2O), 28 (CO) and 44 (CO_2) integrated and quantified using a $CaC_2O_4 \cdot H_2O$ standard. All TG-MS runs were duplicated to ensure reproducibility. Transmission electron microscopy (TEM) images were obtained on a JEOL (model JEM-1400 Plus equipped with an acquisition images camera model GATAN); isopropanol was used as the solvent for exfoliation of 0.1 mg/mL of solid samples using an intensive treatment with an ultrasonic tip (30 W, 2 h with ON-OFF intervals 60-30 s). A drop of the suspension was deposited on a carbon-coated copper grid, evaporating the solvent at room temperature. The XRD profiles were obtained using a Bruker D8-Advance equipment, with Göebel mirror and a step of 0.05º 2θ. The NMR spectra were recorded on a Bruker AC-300 (300 MHz for ^1H) using D_2O as the solvent; chemical shifts are given in δ (parts per million) and coupling constants (*J*) in Hz units. The FT-IR (ATR) spectra were obtained on a Bruker IFS 66/S spectrophotometer equipped with a DLaTGS detector; all the samples were analyzed at room temperature. Mass spectra (EI) were obtained at 70 eV on a Agilent 5975 C of low resolution with a quadrupole analyzer coupled to a gas chromatograph (Agilent7890A), giving relative *m/z* intensities (%).

2.5. Quantum Chemical Simulations

Density Functional Theory (DFT) simulations of key steps in the GO formation process have been carried out using the Gaussian software [43] at the B3LYP/6-31G(d) level [44–46]. Representative model clusters were carefully selected as a judicious compromise between chemical significance, especially regarding electron density at graphene edges, and computational expediency.

3. Results

The powdered and dried dGO sample obtained using the Hummers-Offeman method can be considered as the starting material in the present work. Its characterization results can be compared directly with those of GO reported in the literature, and they are presented first. The TEM images of dGO (Figure 1) reveal the formation of loose and extended GO sheets with an abundance of monolayer planes, corroborated by electron diffraction patterns (see insert in Figure 1c), with high crystallinity and the typical graphene corrugations [47]. Additionally, the presence of OD in the dGO sample is very clear: it is anchored at the GO sheets (see Figure 1 a-b, with different dot sizes), as well as on the lacey support grid (see also Figure 1a-b, dark dots over the grid), indicating that it is prevalent throughout the suspension. On the other hand, Figure S1 shows the XRD of the cGO sample, with an expected sole peak below 10º 2θ, indicative of extensive intercalation that takes place in the majority of the layers, and the abundant monolayers observed by TEM.

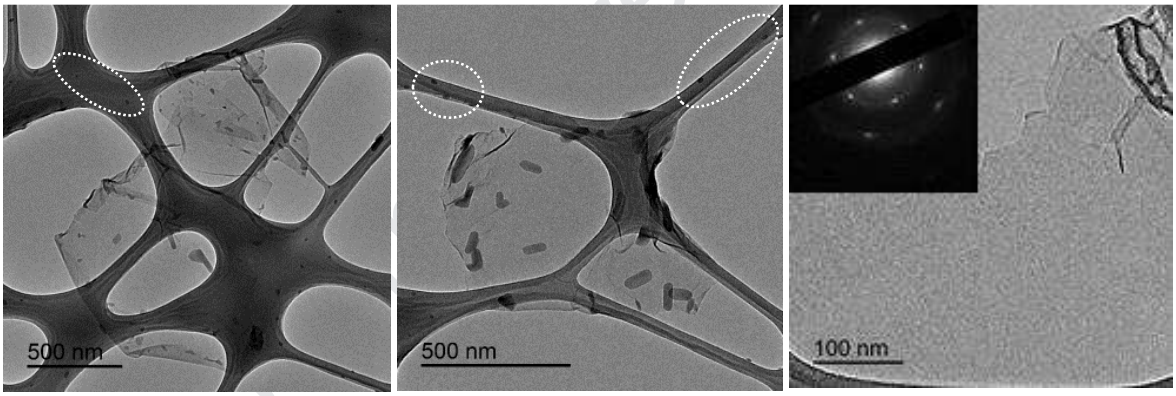

(a) **(b)** **(c)**

Figure 1. (a) and (b) TEM images of initially obtained flat dGO sheets showing the presence of OD over the layers and the lacey grid, and (c) TEM image of a single layer GO according to its electron diffraction pattern (insert).

Figure 2 (see also Figure S2) shows the C1s XPS results for a dGO powdered sample, which are typical for similar samples reported in the literature. Indeed, there is general agreement about assigning C_{1s} binding energies of ca. 284.5 and 289 eV to sp^2 C=C aromatic and sp^2 carboxylic/carboxylate groups, respectively. This is readily verified using model compounds: the benzoic acid spectrum contains only contributions at the above mentioned binding energies [48]. However, there are different interpretations regarding the

285 and 287.6 eV region for graphene-based materials [49–51], even though most uncertainties have been addressed, and largely resolved, in the abundant literature on oxidized carbon fibers [52]: the general rule of thumb is a shift of 1.5 eV per C-O bond. The higher-energy peak corresponds to sp^2 C=O (e.g., quinone, anhydride), and the lower one to C-O or C-O-C (epoxy, ether at ca. 286.3 eV, hydroxyl at 285.6 eV). Using polyethylene terephthalate (PET) as a model compound, the spectrum contains peaks at 286.3 eV and 288.9 eV [53], corresponding to sp^3 C-O-C (ether type) and sp^2 C(O)O, respectively, as expected for its ester functional group, as well as the aromatic sp^2 C=C 284.5 eV peak. Using poly (ether ether ketone) (PEEK) as a model compound the spectrum contains peaks at 286.3 eV (ether) and 287.0 eV (ketone groups) [54]. Typical GO C1s spectra exhibit a clear aromatic peak, and there is another prominent band if the sample is highly oxidized, as evidenced in Figure 2; it typically varies in broadness, symmetry and binding energy location depending on equipment resolution and oxidation level. This brief summary illustrates the challenges in identifying and quantifying even the more abundant groups, and there remains some disagreement in the voluminous literature. Some studies attribute the 286.7 eV peak mainly to C=O groups [7,55], while others assign it mainly to epoxies [56,57]. Consequently, in the absence of careful band deconvolution, the most reliable interpretation remains debatable [58]. What Figure 2 does show is that the dominant oxidized carbon contribution is centered at ca. 286.7 eV, formed by the contribution of different C-O and/or C=O bonds. However, this does not clarify much on its own, in the same manner as 60 ppm signal in 13C-NMR cannot unequivocally indicate the dominant presence of epoxy groups. The minor tail at 289 eV does indicate a minor contribution of carboxyl/carboxylate groups. Identification of lactols can be aided considering carbohydrates as model compounds: there is a 287.5 eV peak assigned to sp^3 carbon bonded to two oxygens [59,60], corresponding to acetal and hemiacetals. This is corroborated using polyoxymethylene (POM) as a model compound, which presents a clear peak at 287.5 eV corresponding to sp^3 carbon bonded to two ether groups [61]. Therefore, 5- and 6-member ring lactones combined with a lactol at graphene edges [18] can also contribute to oxygen surface functionalities at ca. 286.7 eV, in addition to ether, epoxy, phenol and quinone groups.

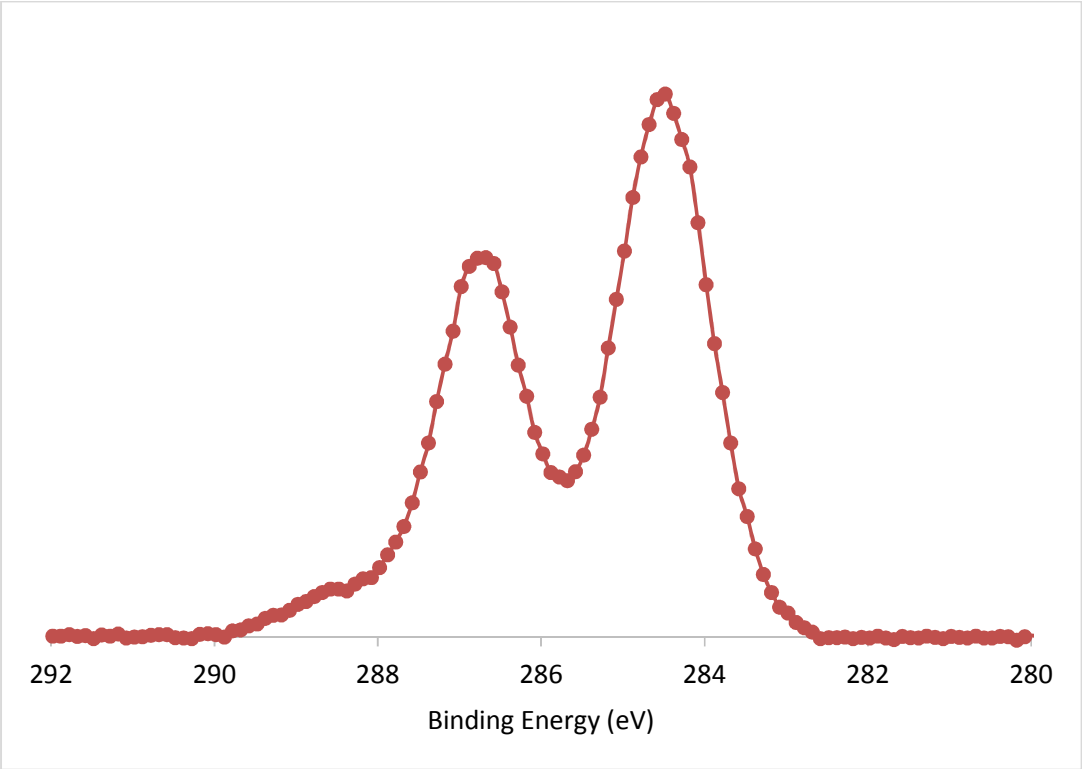

Figure 2. XPS of initially obtained dGO in the C1s range, with clear contributions at 284.5, 286.7 and 289.0 eV. (No deconvolutions are shown due to the debate regarding the multiple origin of the 286.7 eV peak.)

The TG-MS results for dGO, used in its powdered form, are summarized in Figure 3 and Table 1. Figure 3 reveals three characteristic weight loss steps, in agreement with the literature [7,35]. The initial step ranges from room temperature to 140 ºC and corresponds to physisorbed H_2O (*m/z* = 18), around 7% of weight loss. A second weight loss is observed between 140 and 210 ºC, where the quantified signals of m/z = 18, 28 (CO) and 44 (CO_2) are detected, with the amount of CO being considerably lower. The step ranging from 210 to 350 ºC evolved only appreciable amounts of H_2O and CO_2. Eigler *et al.* [62] reported similar non-quantified patterns for H_2O, CO and CO_2, while pointing out the additional evolution of m/z = 64 (SO_2) during the third step, which they attributed to the decomposition of organosulfates. Two important conclusions can be deduced from Table 1: CO_2 evolution is ten times larger than CO evolution; the total mass quantified as H_2O, CO and CO_2 is 45.0 wt-% of the initial GO, and there is still an additional 20% of weight loss registered by TG, which matches to be mostly SO_2 according to the sulfur content

determined by XPS (Table S1). Typical interpretations of surface chemical properties revealed by temperature programmed desorption techniques [63,64] assign carboxyl groups to CO_2 evolution at low temperatures, which is in obvious conflict with our XPS results (Figure 2 shows little contribution of band at 289 eV); furthermore, the decomposition of epoxides is expected to produce CO and at much higher temperatures, and this is not observed in Figure 2. Consequently, the main peak centered at 286.7 eV in Figure 2 is not a fingerprint of basal epoxy (or carbonyl) groups nor does its contribution have to decrease when producing reduced graphene oxide [51,65,66]. If the two-component GO structure is postulated, however, the apparent contradiction is readily resolved: these low-temperature CO_2-CO features in TG-MS and the XPS peak centered at 286.7 eV are evidence for the presence of abundant edge sites in OD, all of them saturated by oxygen complexes such as lactones, lactols and anhydrides. In fact, OD consisting of relatively few benzene rings might decompose entirely as carbon oxides and other volatile hydrocarbons (e.g., acetylene).

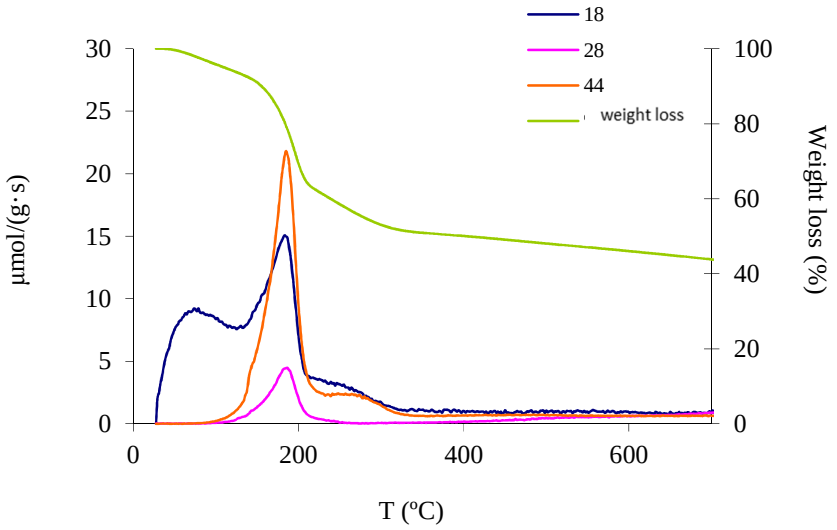

Figure 3. TG-MS of dGO.

Table 1. Quantification of the evolved decomposition products of dGO.

Sample	H_2O (%)	CO (%)	CO_2 (%)	Total by MS (%)	Weight loss by TGA (%)

GO	17.0 ± 0.5	2.6 ± 0.1	25.5 ± 0.6	45.0 ± 1.2	63.2 ± 3.2

The FT-IR spectrum of the initial powdered dGO shows a similar pattern to those available in the literature [67–69]. Above 3000 cm^{-1} there is a broad band that could explain the large amount of H_2O (which agrees with our TG-MS analysis), as well as the presence of functional groups with O-H bonds (ν(O-H)). Furthermore, the band corresponding to C=O at ca. 1750 cm^{-1} (ν(C=O)) corroborates the presence of carboxyl groups and lactones. Also, the presence of aromatic sp^2 C=C in the structure of G-O is corroborated by the signal that appears at 1600 cm^{-1} ((ν(C=C)). Epoxides could be present due to ν_{as}(C-O-C) bands at ca. 1050-1150 cm^{-1} and ν_s(C-O-C) at ca. 840 cm^{-1} [70], and there is an intense signal at 1050 cm^{-1}. However, this signal is much more probably due to asymmetric S=O stretch in organosulfates, since it is clear from XPS and TG-MS that these groups are abundant. Lactols have an asymmetric C-O-C stretch in the 1250-1211 cm^{-1} range, and this would agree with both XPS and TG-MS results.

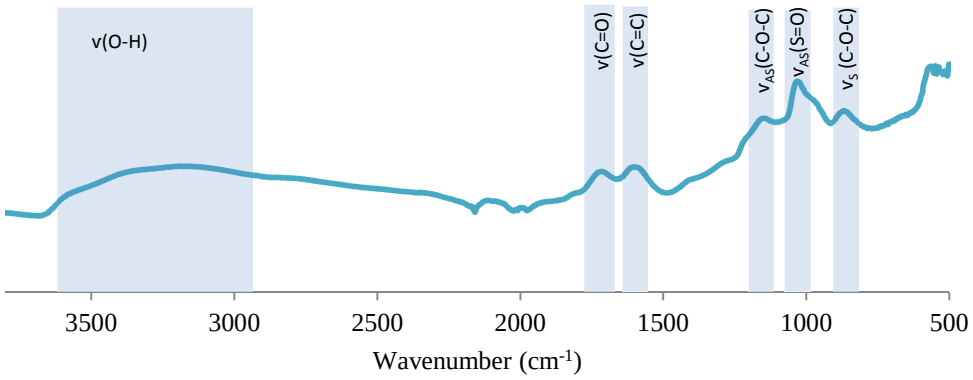

Figure 4. FT-IR of initial powdered dGO.

The results for the base-digested dGO (sonication prior to digestion) and cGO (no sonication used) are particulary noteworthy. Figure 5 shows the gravimetric quantification of the amount of bwGO and OD depending on the treatment and the initial GO used. When dGO digestion was done using NaOH, the yields were 49% bw-dGO_{Na} and 51% OD-dGO_{Na} (calculated by difference), with a negligible amount of the humic-like fraction (hu-

dGO_{Na}). When the same procedure was carried out with cGO, the yield of OD-cGO was only 31%; this undoubtedly indicates that sonication results in fragmentation prior to base digestion [37]. In other words, OD was formed before sonication, and the latter only enhances its formation. This agrees with literature reports that CNT are cut chemically and unraveled when subjected to the Hummers-Offeman treatment [35], as well as with the fact that basal graphite crystals are cleaved when a drop of $KMnO_4/H_2SO_4$ is placed above HOPG [71]. The hu-GO could be quantified upon their isolation by increasing the acidic chatacter of the supernatant solution (below pH 2), and centrifugating the precipitate; however, the yield was too low (see Figure 5). The same procedure was carried out using NH_3 with similar results, which confirms the formation of a larger quantity of OD when sonication was used. In addition, a full gravimetric characterization of the bwGO, hu-GO and fl-GO fractions upon NH_3 digestion shows satisfactory mass balance closure, with a very small contribution of the humic fraction and a very large one of the fulvic fraction. It is also important to note that the high water content of the fulvic fraction is related to the oxygen complexes of fulvic-like compounds, as confirmed by TG-MS (a 30-40% of OD could be water, see Figure 3).

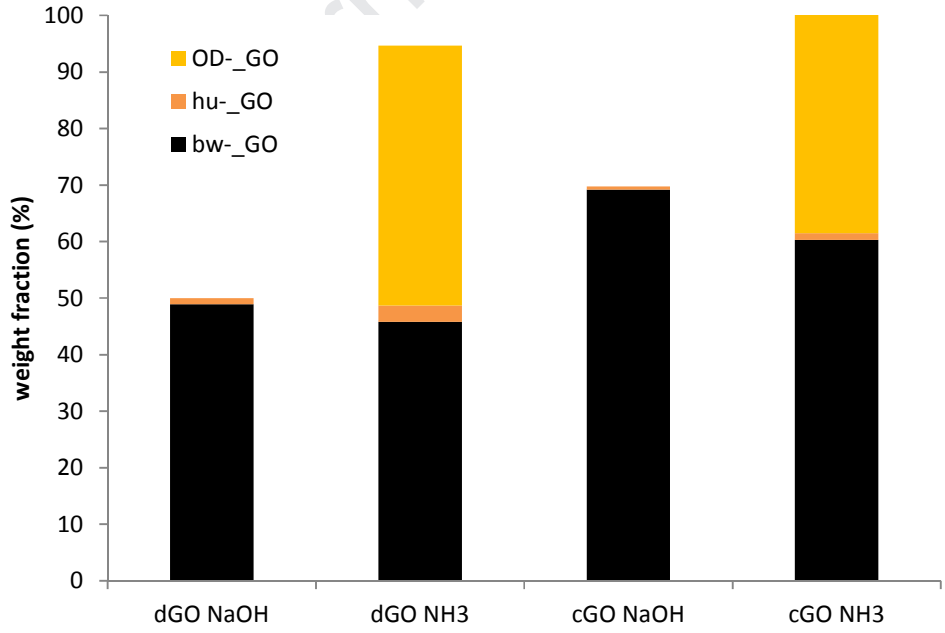

Figure 5. Mass balance of dGO and cGO treated with NaOH or NH_3 (wt% with respect to initial GO).

The TEM images of base-washed materials, humic-like fractions, as well as OD, are shown in Figure 6. No difference was observed when comparing dGO and cGO samples (see also Figure S3). Clean base-washed bwGO sheets are evident and no dots corresponding to OD were found, indicative of its satisfactory removal with either NaOH or NH_3. More wrinkled sheets can be observed when using NaOH in comparison with NH_3 (compare Figure 6 (a) and (b) and Figure S3 (a) and (d)). Dots are observed in images of humic-like fractions with no structure; this is indicative of much smaller sheets (or large molecules) that are highly oxidized (as corroborated by XRD of the hu-dGO_{NaOH}, Figure S1, showing no interlayer registry). Upon focusing the electron beam at high resolution, there was foam-like evidence of sample destruction. Finally, in OD images obtained after NH_3 treatment the absence of lamellar structure and the abundant evidence of dots lead to the conclusion that an aggregation of macromolecules takes place (see Figure S3 (c) and (f)).

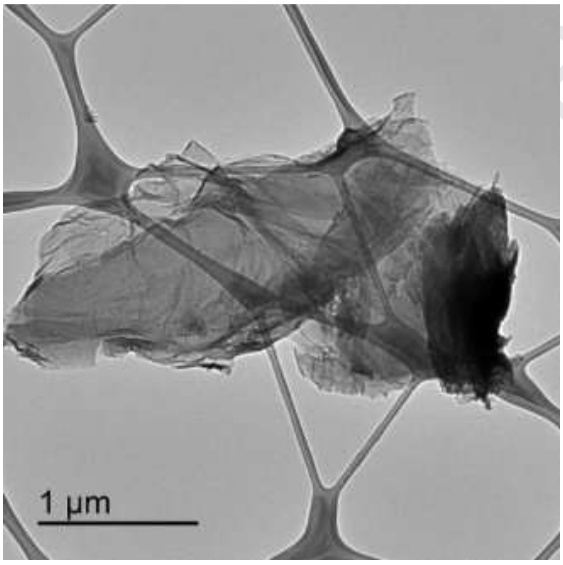

(a)

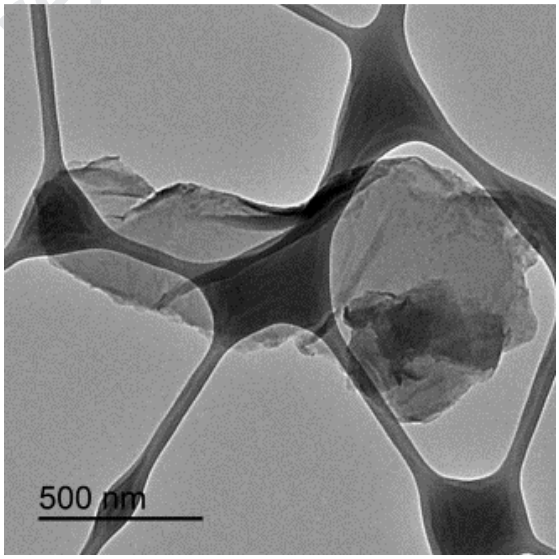

(b)

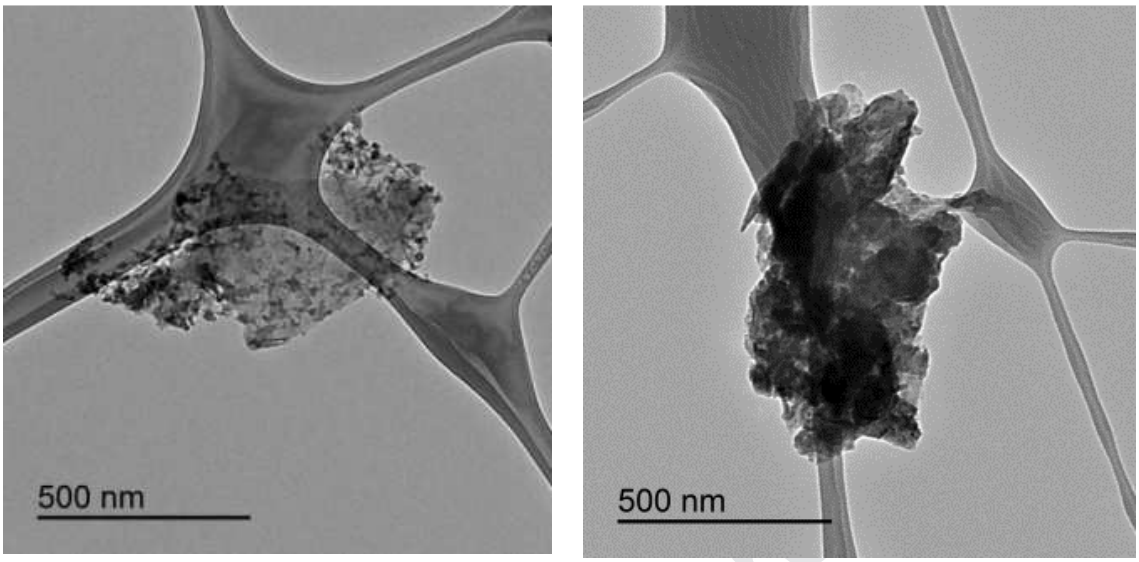

(c) **(d)**

Figure 6. TEM images of (a) bw-dGO$_{NaOH}$, (b) bw-cGO$_{NaOH}$, (c) Hu-dGO$_{NaOH}$ and (d) Hu-cGO$_{NaOH}$ samples.

Figure 7 shows the FT-IR results for the isolated components of dGO and cGO treated with NaOH. The spectra obtained are similar for the corresponding fractions derived from either dGO or cGO. It can be appreciated how the intensity of the peaks corresponding to C=O and C=C decreases and increases, respectively, for bwGO samples with respect to the parent GO. Exactly the opposite occurs for the humic-like fractions; this indicates that the latter lose large graphene sheets, in agreement with the TEM analysis, and with their increase in the abundance of oxygen functionalities. The organosulfate peak also decreases sharply in both bwGO and hu-GO, indicative of their hydrolysis during base digestion. This confirms that GO can be separated into a less oxidized sample (that correspond to bwGO) and a much more oxidized sample (humic-like and fulvic like fractions) after alkaline digestion. In the case of NH_3-washed samples, the intensity changes of C=O and C=C bands are similar (for both dGO and cGO); on the other hand, the spectra are slightly different when compared to NaOH-washed ones due to the expected conversion of carboxyls, lactones and anhydrides into amides (see Figure S4).

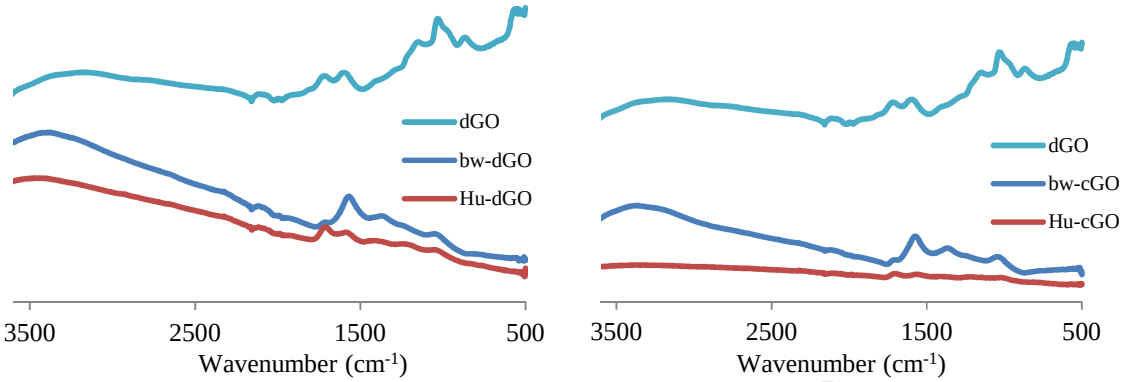

(a) **(b)**

Figure 7. FT-IR spectra of (a) dGO, bw-dGO$_{NaOH}$, Hu-dGO$_{NaOH}$ samples and (b) dGO, bw-cGO$_{NaOH}$, Hu-cGO$_{NaOH}$ samples.

When the same samples were examined by XPS, the spectra obtained were very similar regardless of the initial dGO (Figure 8) or cGO (Figure S5), thus reinforcing our conclusions from FT-IR and TEM evidence. The bw-dGO$_{NaOH}$ is a much less oxidized sample, with a sharply reduced 286.7 eV peak and a nearly intact carboxyl group contribution at 289 eV (Figure 8a). Surprisingly, a similar pattern is observed for sample Hu-dGO$_{NaOH}$ (Figure 8c), with the 286.7 eV peak being slightly stronger due to its high edge-to-basal plane ratio; if in starting dGO this were mainly due to basal epoxide, it would be unrealistic to lose these functionalities when removing the smaller sheets, since larger sheets would be fully decorated with epoxides. In contrast, it would be expected that the carboxyl groups are lost when removing such sheets if only these groups were at the GO edges. Thus, it is confirmed here that the 286.7 eV contribution should not be attributed to epoxies, in agreement with the rule of thumb established in the carbon fibers literature [52], but to cyclic lactones combined with lactols along the edges of the OD component of GO.

Organosulfates were hydrolyzed in the base digestion, and therefore bwGO and hu-GO do not show sulfur contents above 0.1% (see Table S2). And in the NH_3-washed samples (Figure 8b, 8d, 8e, see also Figure S5) the contribution of carboxyls in bwGO decreases with respect to initial dGO, almost disappearing completely. The broad peak at ca. 286.7 eV increases with respect to its NaOH-treated counterpart, indicating the formation of new C-N bonds (see also XPS composition results in Table S2). The Hu-GO$_{NH3}$ sample

exhibited similar behavior to that observed for $bwGO_{NH3}$, with a more pronounced 286.5 eV peak reflecting its high edge to basal plane ratio, with C-N functionalities at the edges. However, in the case of OD (both fulvic- and humic-like fractions) the large proportion of carboxylic/carboxylate groups is due to the fulvic-like fraction and oxygen functionalities (and thus low carbon content in comparison with bw-GO), and thus it is a reflection of its small sheet size and high edge site density; the OD also has rather high sulfur and nitrogen contents, presumably due to a significant amount of condensed ammonium sulfate.

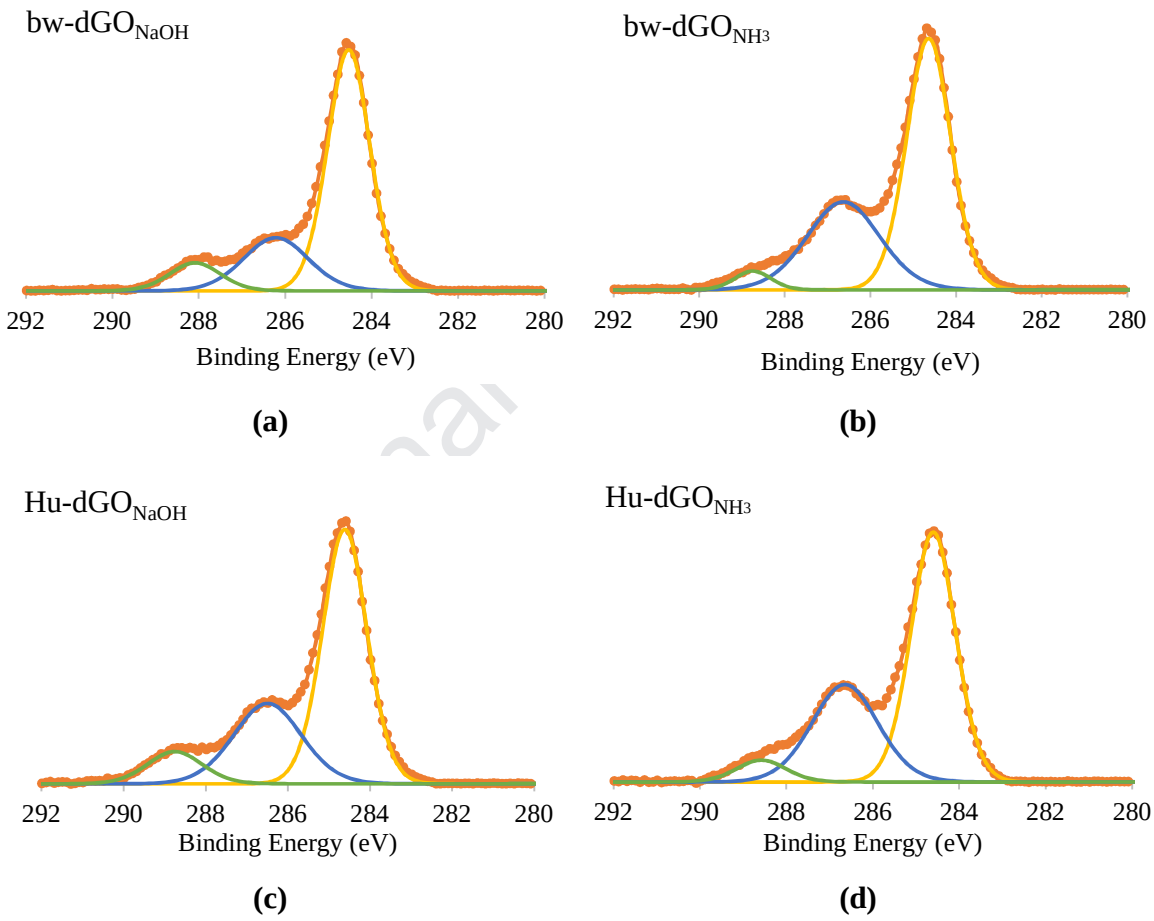

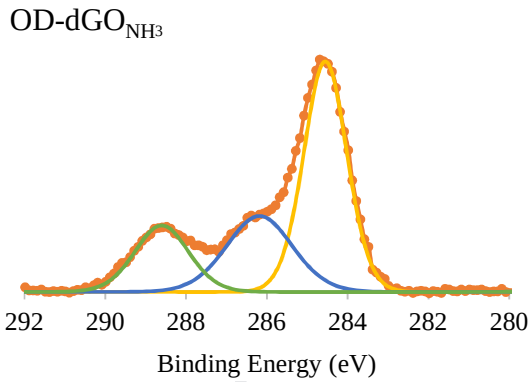

(e)

Figure 8. XPS C1s spectra of (a) bw-dGO$_{NaOH}$, (b) bw-dGO$_{NH3}$, (c) Hu-dGO$_{NaOH}$, (d) Hu-dGO$_{NH3}$, (e) OD-dGO$_{NH3}$. (XPS spectra were decolvoluted to Gaussian peaks at 284.5, 286.7 and 289 eV.)

Figure 9 shows the TG-MS plots corresponding to bw-GO derived from both dGO and cGO in NaOH and NH_3 digestions, which are very different from that of parent dGO (Figure 3). Sample bw-dGO$_{NaOH}$ (Figure 9a) presents a surprising thermogram with a continuous and nearly linear weight loss with increasing temperature (no steps), whereas bw-cGO$_{Na}$ (Figure 9b) does show a clear step below 200 ºC (although not as pronounced in comparison with Figure 3) and a similar monotonic weight loss. There is again an initial loss of physisorbed H_2O, but there is no evolution of CO in the second step (140–200 ºC); above 200 ºC there is continuous CO_2 evolution, a completely different pattern with respect to Figure 3, where CO_2 evolution essentially ended at 300 ºC. Absence of CO evolution indicates absence of hydroxyl, epoxy, ether and even anhydride groups. Additionally, it cannot be attributed exclusively to carboxyl groups (not negligible in bw-cGO$_{NaOH}$) since their dominant evolution occurs over the entire temperature range. Therefore, cyclic lactone and/or lactol groups of different thermal stability (e.g., different ring sizes) located at GO edges offer the most logical explanation for this anomalous TG-MS pattern. In the case of NH_3-washed bw-GO samples (Figure 9c and 9d), a pattern more similar to parent dGO is observed, with a pronounced weight loss just below 200 ºC, with evolution of H_2O, CO_2 and some CO. As mentioned above, formation of new C-N bonds with those parent lactone and lactol groups takes place and therefore the decomposition of these samples takes a different course.

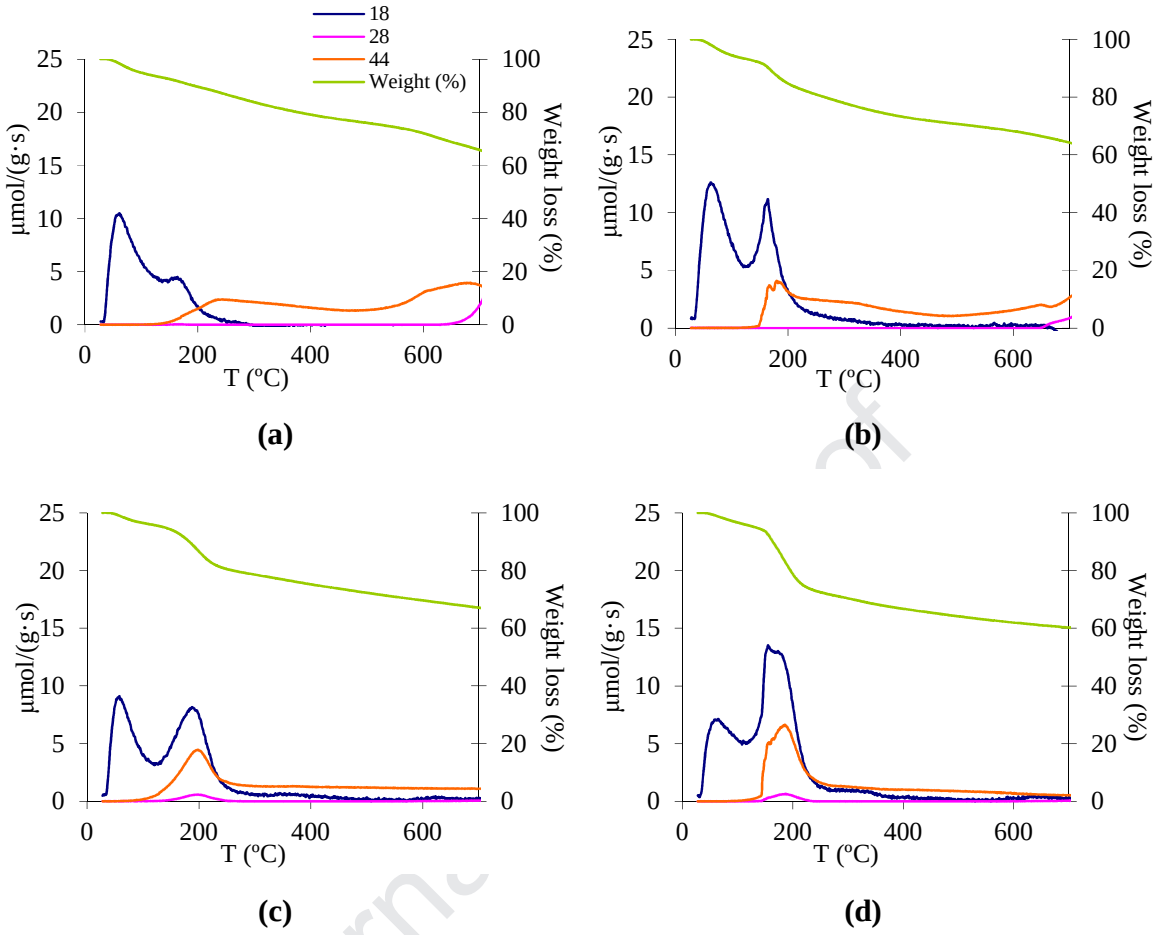

Figure 9. TG-MS of (a) bw-dGO$_{NaOH}$, (b) bw-cGO$_{NaOH}$, (c) bw-dGO$_{NH_3}$ and (d) bw-cGO$_{NH_3}$ samples.

An important issue is noteworthy upon quantification of H_2O, CO and CO_2, as summarized in Table 2. For all bwGO samples, the total amount determined by mass spectrometry matches the total weight loss determined by TG. Similar results were obtained in all the cases (see Figure S6) for the fraction corresponding to hu-GO. As there were no organosulfates present (confirmed by XPS), this implies that most of the weight loss can be accounted for by edge-bound lactol-type complexes, which must be mainly at graphene edges and whose decomposition produces CO_2.

Table 2. Quantification of the evolved decomposition products in bw-GO samples.

	H_2O	CO	CO_2	Mass	Weight

	%	%	%	detected by MS %	loss by TG %
bw-dGO$_{NaOH}$	8.9 ± 0.5	0	20.6 ± 0.6	29.5 ± 1.2	28 ± 0.6
bw-cGO$_{NaOH}$	16.1 ± 0.8	0	21.9 ± 0.6	37.9 ± 1.4	32 ± 0.6
bw-dGO$_{NH3}$	13.5 ± 0.5	0.6 ± 0.1	20.2 ± 0.6	33.7 ± 1.2	30.5 ± 0.7
bw-cGO$_{NH3}$	17.3 ± 0.6	0.6 ± 0.1	21.2 ± 0.6	38.5 ± 1.3	38.0 ± 0.7

Finally, TG-MS results corresponding to the OD fractions in NH_3-washed samples were analyzed upon their isolation after rotovapor water evaporation. A very different pattern emerged with respect to previously analyzed samples. Very little carbon oxides evolved when compared to water evolution; carbon content was only 26% according to XPS (Table S2), and only measurable CO_2 evolved with peaks at 180ºC (as parent dGO and bw-dGO$_{NH3}$) and 350 ºC, which was not observed with previous samples. There are two large and sudden steps in H_2O evolution at ca. 250 and 320 ºC. During the evaporation step, when OD was isolated, hydrolyzed organosulfates formed $(NH_4)_2SO_4xH_2O$ precipitates, plus some trapped ammonia (N content in OD was 16% according to XPS, Table S2); the weight loss at ~180 ºC is mainly attributable to trapped NH_3, at 250 ºC the H_2O evolved is assigned to the dehydration of the ammonium salt and the main weight loss at ~340 ºC is due to its decomposition. As shown in Figure 5, bw-GO$_{NH3}$ gravimetric yield was around 45 and 60% for dGO and cGO, respectively, and OD$_{NH3}$ yields were 46 and 40%, which indicates very good mass balance closure with respect to parent dGO or cGO prior to ammonia digestion. However, in OD decomposition we recorded a high content of H_2O bonded to extensively oxidized carbon, plus abundant presence of salts derived from parent organosulfate groups. This confirms the formation of GO characterized by clean, slightly oxidized bwGO sheets as well as more oxidized moieties in the range of molecular sizes.

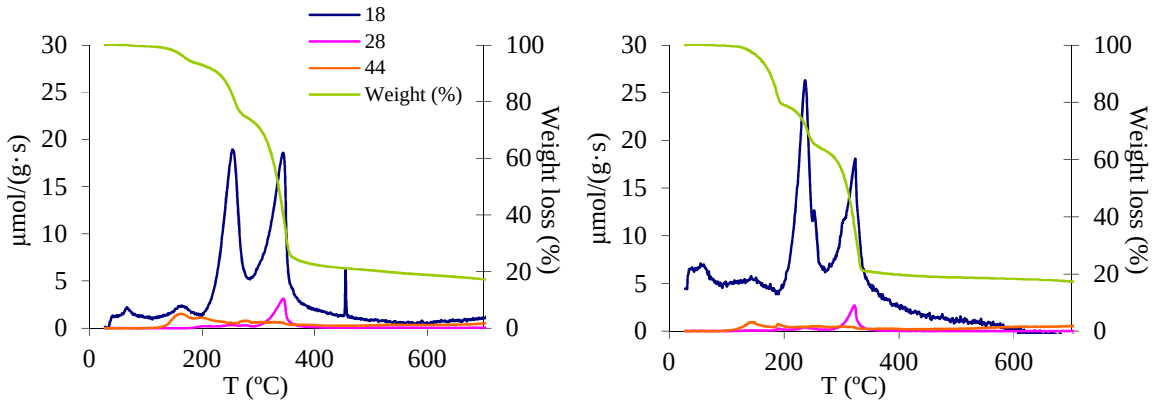

Figure 10. TG-MS of (a) OD-dGO$_{NH_3}$ and (b) OD- cGO$_{NH_3}$ samples.

The fulvic-like fraction of NaOH-derived OD could not be isolated for gravimetric characterization, since it resides in water solution with high NaCl concentration. An attempt was made to extract some fulvic acids after removing the solid hu-GO$_{NaOH}$ fraction by centrifugation. The solution was evaporated in vacuum and, once the sample was dried, the organic components were extracted with ethanol; the ethanol was then removed and the resulting pale yellow oil was analyzed by CG-MS and ^{1}H-NMR (see Figure S7). This provided evidence for the presence of phthalates that could not be detected before ethanol extraction using the same type of analysis. We can thus conclude that the precursors in the formation of phthalates are very likely cyclic lactols, anhydrides and/or lactones. Once again such carboxylic functionalities seem to be present in the dGO sample.

4. Discussion

By combining the results of a battery of complementary experimental techniques with insights from DFT analysis, remarkably consistent mechanistic patterns in graphite-to-graphene oxide conversion are now emerging. And they agree with expected trends that are reasonably well understood on the basis of surface chemical behavior of sp^2-hybridized carbon materials ranging from coal or activated carbon to carbon black or graphite. The main chemical features of the graphene-based structures that are formed in this process are shown in Figure 11.

Graphene oxide is normally produced from flake graphite (FG) or its parent expanded graphite (EG), which is a macrocrystalline material when separated by flotation and subsequently thermally purified and partially exfoliated [72]. This elongated and layered material has a broad particle size distribution [73] and contains many structural defects caused by its natural formation. In the classical Hummers-Offeman methodology, it is therefore easily intercalated with anhydrous or highly concentrated H_2SO_4. The Mn_2O_7 dimer (more reactive than permanganate itself) attacks primarily those defects, as well as edge sites, both external (at graphene edges) and internal (e.g., vacancies), and not the aromatic structure in the basal plane [74]. This yields pristine graphite oxide (pGO) whose flakes remain essentially intact [4]; the most often cited oxygen surface groups in this intermediate product are quinones, organosulfates and some sp^3 C-O groups [5,75]. Be that as it may, the crucial issues regarding the final structure of graphene oxide, and the emergence of its two components, are the relative importance of transfer of one *vs.* two oxygen atoms to the carbon active sites and the resulting fate of quinone *vs.* peroxy *vs.* dioxiranyl surface functionalities. Of greatest relevance here, as discussed below, are the facts that (i) both nitrate and peroxide are 1O-transfer oxidants whereas permanganate is a 2O-transfer oxidant [44], and (ii) the origin of the widely acknowledged (and crucial) presence of epoxy groups on the basal plane [76] has not received the scrutiny that it deserves.

The principal oxidation steps, which are diffusion-controlled [4,77] occur upon pouring sulfuric acid-containing suspension into water. These reactions can be minimized only if the temperature is kept low (say, below 10 ^{o}C), e.g., if a very gradual H_2O addition dissipates effectively the resulting heat of mixing [78]. Figures S8 and S9 show the C1s XPS and TG-MS, respectively, of eGO sample and confirm that most oxidation reactions are mitigated when the temperature is kept below 10 ºC when adding water. The controlled action of permanganate anions is the key step here [35,67,79] but heretofore its essential details have been elusive. In particular, it is contrary to detailed and voluminous experimental evidence to assume that oxygen transfer occurs on defect-free basal plane [80,81], either curved [35,82–84] or flat [4,83,85,86]; indeed, the putative decoration of these new unzipped edges with quinone or phenol oxygen functionalities [39,87–91]

implies that the desorption (TG-MS) spectrum would be dominated by high-temperature evolution of CO [92–94], which is clearly not the case (see Figure 3). Furthermore, this is contrary to the observation [4] that the "conversion … to an oxidized form of graphite [occurs by virtue of] an edge-to-centre propagation of oxygen functionalities" [95]. And once the epoxy groups [85] reach the basal plane by spillover from graphene edges [45], it remains to be demonstrated how the propagation of underlying C-C bond cleavage [85,86] actually occurs in the presence of a 2O-transfer agent such as permanganate; indeed, oxygen insertion into the basal plane ('unzipping') does not necessarily lead to scissor-like cutting of graphene sheets.

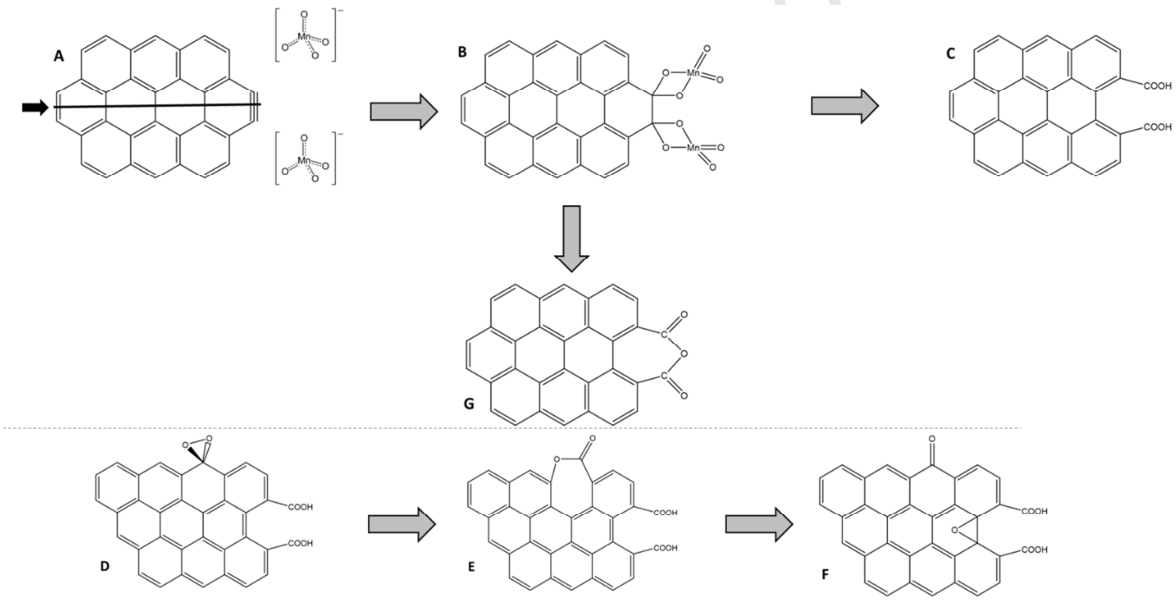

Figure 11. Representative graphene moieties on the mechanistic path from graphite to two-component GO (early stage of the scissor-cut mechanism).

As summarized in Figure 11, our results allow us to postulate the following sequence of events. Once MnO_4^- anions or Mn_2O_7 are able to diffuse between the graphene layers upon H_2SO_4-mediated graphite expansion, oxygen transfer at the active sites can proceed by two paths: (i) At the zigzag site [44], a dioxiranyl functionality (structure D) is a precursor to oxygen insertion and formation of a seven-membered cyclic lactone (structure E). (ii) At the armchair site a similar intermediate (structure B) initiates the chemical scissors effect

[96], as the C-C bond is broken in a highly exothermic process -- e.g., 268 kcal/mol at the carbyne-type [46] site in $C_{32}H_{12}$ (structure A). This results in the formation of adjacent carboxyl groups (structure C); the DFT-optimized geometry of this model cluster, with its characteristic tearing/bending feature, is shown in Figure 12. These intermediate structures B and D, generated during the formation of pGO, will propagate quicky in a chemical scissor process after pouring water and its consequent temperature increase, ultimately resulting in structure F.

Once initiated, as argued above, the propagation of the chemical scissors effect has not received the attention that it deserves, nor has its obvious relationship to the extensively investigated oxidative unzipping of CNTs. Thus, for example, while the formation of a manganate ester on a basal-plane site has been shown (hydrogen peroxide might also promote this), perhaps surprisingly, to be moderately exothermic [82], the necessary oxygen insertion in the basal plane is much more difficult than at the graphene edge (structure F formed via structure E [45]). And, therefore, a cooperative effect of epoxy and oxiranyl groups summarized in Figures 11 and 12 emerges as the most feasible mechanistic path consistent both with our experimental results and general knowledge of carbon surface chemistry [44–46]. The graphene oxide sheets resulting from further tearing of structure F have a very broad size distribution, ranging from μm (such as bwGO) to the nanoscale, including the size of organic molecules (such as OD). Most of the oxygen functionalities are thus located at the edges, where dioxiranyls (in 2O-transfer) are prone to stabilization as cyclic lactones/lactols (i.e., oxepinones) and anhydrides (structures E and G in Figure 11). Thus, for example, lactones are produced readily when H_2O_2 is added in the third step (see Figure 12).

As a consequence, typical XPS patterns of GO confirm that the larger sheets are covered by OD, with the main band at ca. 286.7 eV being due to lactol groups. Indeed, there is increasing HRTEM evidence [97] for such presence of 7-membered rings in GO. Our TG-MS and FT-IR spectra also indicate the dominant contribution of lactones/lactols and anhydrides, with CO_2 evolving primarily below 250 ^{o}C, which is not compatible with a dominant presence of epoxies on the basal plane. As illustrated in Section 3, the evidence

for the presence of epoxies hinges on one-sided interpretation of the 13C-NMR results (signal at ca. 60 ppm); the same feature is also present in the classical structure of coals and other geo-organic materials and it is attributed there to methoxyl groups [98,99]. Furthermore, when analyzing the fractions separated by NaOH digestion based on their pH stability, according to molecular/layer size, the larger sheets had a much lower lactone/lactol population. At the same time, TG-MS results indicated that the residual lactones/lactols have a range of thermal stabilities. This is indeed to be expected, on the basis of their widely varying chemical environments at both zigzag and armchair graphene edges, the most emblematic of which have been succinctly represented in Figure 11.

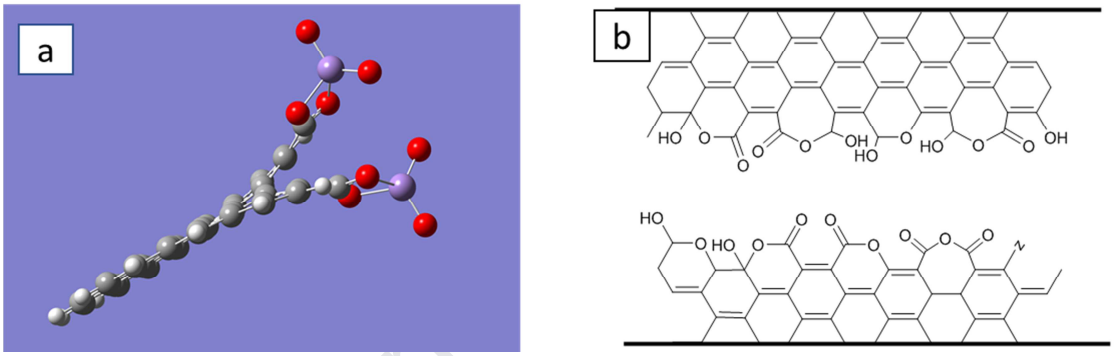

Figure 12. (a) Optimized geometry of $C_{32}H_{12}(MnO_4)_2$ which initiates the chemical scissors effect, and (b) schematic representation of the final structure resulting upon GO cutting.

5. Conclusions

Many important details regarding graphene oxide preparation and structure are too often made obscure due to inadequate characterization and interpretation of its chemical surface properties. Our results point to graphene oxide formation being a process that is mechanistically consistent with all the other oxygen-transfer processes (e.g. carbon gasification, graphene functionalization, oxygen reduction reaction); they also show that oxidative debris is produced prior to base digestion. Its formation, enhanced by sonication, is a consequence of the chemical scissors effect of permanganate anions in the basal plane facilitated by sulfuric acid as exfoliant and solvent. The last step in the Hummers-Offeman

graphite oxide synthesis (contact with aqueous H_2O_2) promotes the stabilization of graphene edge sites as both quinone groups and oxepinone-type surface functionalities in crystallites that have a broad distribution of sizes. These groups are the dominant ones in graphene oxide, as evidenced from a combined examination of our own XPS, FT-IR and TG-MS results, as well as those widely reported in the literature. Consequently, epoxy groups, which do play a role in the unzipping of the basal plane, are not dominant on the graphene oxide surface. Cleaning the graphene oxide during base digestion produces the separation of large and small sheets, yielding an enriched fraction of large sheets, with little surface oxygen since those functionalities are mainly at their edges. Addtionally, base digestion and subsequent reprotonation hydrolyzes some of the lactone groups to carboxylic acids.

Acknowledgements

The authors gratefully acknowledge the financial support of the Ministerio de Economía y Competitividad of Spain, MINECO (Project CTQ2013-44213-R), and Generalitat Valenciana (project PROMETEOII/2014/007). LRR is grateful for the support of CONICYT-Chile (project Fondecyt 1160949).

References

[1] Dreyer DR, Park S, Bielawski CW, Ruoff RS, The chemistry of graphene oxide, Chem. Soc. Rev. 39 (2010) 228–240. http://dx.doi.org/10.1039/B917103G.

[2] Hummers WS, Offeman RE, Preparation of Graphitic Oxide, J. Am. Chem. Soc. 80 (1958) 1339–1339. doi:10.1021/ja01539a017.

[3] Marcano DC, Kosynkin D V., Berlin JM, Sinitskii A, Sun Z, Slesarev A, et al., Improved Synthesis of Graphene Oxide, ACS Nano. 4 (2010) 4806–4814. doi:10.1021/nn1006368.

[4] Dimiev AM, Tour JM, Mechanism of Graphene Oxide Formation, ACS Nano. 8

(2014) 3060–3068. doi:10.1021/nn500606a.

[5] Eigler S, Graphite sulphate - a precursor to graphene, Chem. Commun. 51 (2015) 3162–3165. doi:10.1039/c4cc09381j.

[6] Kang JH, Kim T, Choi J, Park J, Kim YS, Chang MS, et al., Hidden Second Oxidation Step of Hummers Method, Chem. Mater. 28 (2016) 756–764. doi:10.1021/acs.chemmater.5b03700.

[7] Stankovich S, Dikin DA, Piner RD, Kohlhaas KA, Kleinhammes A, Jia Y, et al., Synthesis of graphene-based nanosheets via chemical reduction of exfoliated graphite oxide, Carbon. 45 (2007) 1558–1565. http://www.scopus.com/inward/record.url?eid=2-s2.0-34249742469&partnerID=40&md5=87511fba173e2a553ddbb3370c3548fe.

[8] Yoo MJ, Park HB, Effect of hydrogen peroxide on properties of graphene oxide in Hummers method, Carbon. 141 (2019) 515–522. doi:10.1016/J.CARBON.2018.10.009.

[9] Shin Y-R, Jung S-M, Jeon I-Y, Baek J-B, The oxidation mechanism of highly ordered pyrolytic graphite in a nitric acid/sulfuric acid mixture, Carbon. 52 (2013) 493–498. doi:http://dx.doi.org/10.1016/j.carbon.2012.10.001.

[10] Hofmann U, Holst R, Über die Säurenatur und die Methylierung von Graphitoxyd, Berichte Der Dtsch. Chem. Gesellschaft (A B Ser. 72 (1939) 754–771. doi:10.1002/cber.19390720417.

[11] Scholz W, Boehm HP, Untersuchungen am Graphitoxid. VI. Betrachtungen zur Struktur des Graphitoxids, Zeitschrift Für Anorg. Und Allg. Chemie. 369 (1969)

327–340. doi:10.1002/zaac.19693690322.

[12] Lerf A, He H, Forster M, Klinowski J, Structure of Graphite Oxide Revisited [I], J. Phys. Chem. B. 102 (1998) 4477–4482. doi:10.1021/jp9731821.

[13] Bagri A, Mattevi C, Acik M, Chabal YJ, Chhowalla M, Shenoy VB, Structural evolution during the reduction of chemically derived graphene oxide, Nat. Chem. 2 (2010) 581–587. doi:10.1038/nchem.686.

[14] Mermoux M, Chabre Y, Rousseau A, FTIR and 13C NMR study of graphite oxide, Carbon. 29 (1991) 469–474. http://www.sciencedirect.com/science/article/pii/0008622391902166.

[15] Haubner K, Morawski J, Olk P, Eng LM, Ziegler C, Adolphi B, et al., The route to functional graphene oxide, (n.d.). doi:10.1002/cphc.200.

[16] Pei S, Cheng H-M, The reduction of graphene oxide, Carbon. (2011). http://www.sciencedirect.com/science/article/pii/S0008622311008967.

[17] Mattevi C, Eda G, Agnoli S, Miller S, Mkhoyan KA, Celik O, et al., Evolution of electrical, chemical, and structural properties of transparent and conducting chemically derived graphene thin films, Adv. Funct. Mater. 19 (2009) 2577–2583. http://www.scopus.com/inward/record.url?eid=2-s2.0-70349231471&partnerID=40&md5=469bb20bc0600f287a2cbae037a081de.

[18] Gao W, Alemany LB, Ci L, Ajayan PM, New insights into the structure and reduction of graphite oxide, Nat Chem. 1 (2009) 403–408. doi:http://www.nature.com/nchem/journal/v1/n5/suppinfo/nchem.281_S1.html.

[19] Dimiev A, Kosynkin D V, Alemany LB, Chaguine P, Tour JM, Pristine graphite

oxide, J. Am. Chem. Soc. 134 (2012) 2815–2822. http://www.scopus.com/inward/record.url?eid=2-s2.0-84856750329&partnerID=40&md5=414728d4b78126f3ceb4eb9e8581d029.

[20] Rourke JP, Pandey PA, Moore JJ, Bates M, Kinloch IA, Young RJ, et al., The Real Graphene Oxide Revealed: Stripping the Oxidative Debris from the Graphene-like Sheets, Angew. Chemie Int. Ed. 50 (2011) 3173–3177. doi:10.1002/anie.201007520.

[21] Hummers W, Offeman R, Preparation of graphitic oxide, J. Am. Chem. Soc. 80 (1958) 1339.

[22] Juettner B, Mellitic Acid from Coals, Cokes and Graphites, J. Am. Chem. Soc. 59 (1937) 208–213. doi:10.1021/ja01280a052.

[23] Juettner B, Smith RC, Howard HC, Oxidation of a Pittsburgh Seam Bituminous Coal and Low Temperature Coke by Alkaline Permanganate, J. Am. Chem. Soc. 59 (1937) 236–241. doi:10.1021/ja01281a006.

[24] Thiele H, Über Salzbildung und Basenaustausch der Graphitsäure, Kolloid-Z. 80 (1937) 1–20.

[25] Lerf A, Graphite Oxide Story - From the Beginning Till the Graphene Hype, in: A. Dimiev, S. Eigler (Eds.), Graphene Oxide Fundam. Appl., Wiley, 2016: pp. 1–35. doi:10.1002/9781119069447.ch1.

[26] Fogden S, Verdejo R, Cottam B, Shaffer M, Purification of single walled carbon nanotubes: The problem with oxidation debris, Chem. Phys. Lett. 460 (2008) 162–167. doi:10.1016/j.cplett.2008.05.069.

[27] Verdejo R, Lamoriniere S, Cottam B, Bismarck A, Shaffer M, Removal of oxidation

debris from multi-walled carbon nanotubes, Chem. Commun. (2007) 513–515. doi:10.1039/B611930A.

[28] Salzmann CG, Llewellyn SA, Tobias G, Ward MAH, Huh Y, Green MLH, The Role of Carboxylated Carbonaceous Fragments in the Functionalization and Spectroscopy of a Single-Walled Carbon-Nanotube Material, Adv. Mater. 19 (2007) 883–887. doi:10.1002/adma.200601310.

[29] Wu Z, Pittman Jr CU, Gardner SD, Nitric acid oxidation of carbon fibers and the effects of subsequent treatment in refluxing aqueous NaOH, Carbon. 33 (1995) 597–605. doi:http://dx.doi.org/10.1016/0008-6223(95)00145-4.

[30] Thomas HR, Valles C, Young RJ, Kinloch IA, Wilson NR, Rourke JP, Identifying the fluorescence of graphene oxide, J. Mater. Chem. C. 1 (2013) 338–342. doi:10.1039/c2tc00234e.

[31] Rodriguez-Pastor I, Ramos-Fernandez G, Varela-Rizo H, Terrones M, Martin-Gullon I, Towards the understanding of the graphene oxide structure: How to control the formation of humic-and fulvic-like oxidized debris, Carbon. 84 (2015) 299–309. doi:10.1016/j.carbon.2014.12.027.

[32] Faria AF, Martinez DST, Moraes ACM, Maia Da Costa MEH, Barros EB, Souza Filho AG, et al., Unveiling the role of oxidation debris on the surface chemistry of graphene through the anchoring of Ag nanoparticles, Chem. Mater. 24 (2012) 4080–4087. doi:10.1021/cm301939s.

[33] Dimiev AM, Polson TA, Contesting the two-component structural model of graphene oxide and reexamining the chemistry of graphene oxide in basic media,

Carbon. 93 (2015) 544–554. doi:http://dx.doi.org/10.1016/j.carbon.2015.05.058.

[34] Naumov A, Grote F, Overgaard M, Roth A, Halbig CE, Nørgaard K, et al., Graphene Oxide: A One- versus Two-Component Material, J. Am. Chem. Soc. 138 (2016) 11445–11448. doi:10.1021/jacs.6b05928.

[35] Kosynkin D V., Higginbotham AL, Sinitskii A, Lomeda JR, Dimiev A, Price BK, et al., Longitudinal unzipping of carbon nanotubes to form graphene nanoribbons, Nature. 458 (2009) 872–876. doi:10.1038/nature07872.

[36] Dimiev AM, Khannanov A, Vakhitov I, Kiiamov A, Shukhina K, Tour JM, Revisiting the Mechanism of Oxidative Unzipping of Multiwall Carbon Nanotubes to Graphene Nanoribbons, ACS Nano. 12 (2018) 3985–3993. doi:10.1021/acsnano.8b01617.

[37] Liscio A, Kouroupis-Agalou K, Betriu XD, Kovtun A, Treossi E, Pugno NM, et al., Evolution of the size and shape of 2D nanosheets during ultrasonic fragmentation, 2D Mater. 4 (2017) 025017. doi:10.1088/2053-1583/aa57ff.

[38] Aliyev E, Filiz V, Khan MM, Lee YJ, Abetz C, Abetz V, Structural Characterization of Graphene Oxide: Surface Functional Groups and Fractionated Oxidative Debris, Nanomaterials. 9 (2019) 1180. doi:10.3390/nano9081180.

[39] Dionizio Moreira M, Coluci VR, Initial stages of graphene oxide cracking in basic media, Carbon. 142 (2019) 217–223. doi:10.1016/j.carbon.2018.10.037.

[40] Qiao Q, Liu C, Gao W, Huang L, Graphene oxide model with desirable structural and chemical properties, Carbon. 143 (2019) 566–577. doi:10.1016/j.carbon.2018.11.063.

[41] Thomas HR, Day SP, Woodruff WE, Vallés C, Young RJ, Kinloch IA, et al., Deoxygenation of Graphene Oxide: Reduction or Cleaning? _SI, Chem. Mater. (2013) 1–16.

[42] Eigler S, Grimm S, Hof F, Hirsch A, Graphene oxide: a stable carbon framework for functionalization, J. Mater. Chem. A. 1 (2013) 11559–11562. doi:10.1039/c3ta12975f.

[43] Frisch, Trucks G, Schlegel H, Scuseria G, Robb M, Cheeseman J, et al., Gaussian 03, Revision C.02, (2004).

[44] Radovic LR, Mora-Vilches C V., Salgado-Casanova AJA, Buljan A, Graphene functionalization: Mechanism of carboxyl group formation, Carbon. 130 (2018) 340–349. doi:10.1016/j.carbon.2017.12.112.

[45] Radovic LR, Silva-Tapia AB, Vallejos-Burgos F, Oxygen migration on the graphene surface. 1. Origin of epoxide groups, Carbon. 49 (2011) 4218–4225. doi:10.1016/J.CARBON.2011.05.059.

[46] Radovic LR, Bockrath B, On the chemical nature of graphene edges: Origin of stability and potential for magnetism in carbon materials, J. Am. Chem. Soc. 127 (2005) 5917–5927. doi:10.1021/ja050124h.

[47] Meyer JC, Geim AK, Katsnelson MI, Novoselov KS, Booth TJ, Roth S, The structure of suspended graphene sheets, Nature. 446 (2007) 60–63. doi:http://www.nature.com/nature/journal/v446/n7131/suppinfo/nature05545_S1.html.

[48] Kreil J, Ellingsworth E, Szulczewski G, X-ray photoelectron spectroscopy study of

para-substituted benzoic acids chemisorbed to aluminum oxide thin films, J. Vac. Sci. Technol. A. 31 (2013) 6–107. doi:10.1116/1.4824166.

[49] Compton OC, Jain B, Dikin DA, Abouimrane A, Amine K, Nguyen ST, Chemically Active Reduced Graphene Oxide with Tunable C/O Ratios, ACS Nano. 5 (2011) 4380–4391. doi:10.1021/nn1030725.

[50] Larciprete R, Gardonio S, Petaccia L, Lizzit S, Atomic oxygen functionalization of double walled C nanotubes, Carbon. 47 (2009) 2579–2589. doi:http://dx.doi.org/10.1016/j.carbon.2009.05.008.

[51] Ganguly A, Sharma S, Papakonstantinou P, Hamilton J, Probing the Thermal Deoxygenation of Graphene Oxide Using High-Resolution In Situ X-ray-Based Spectroscopies, J. Phys. Chem. C. 115 (2011) 17009–17019. doi:10.1021/jp203741y.

[52] Yumitori S, Correlation of C 1s chemical state intensities with the O 1s intensity in the XPS analysis of anodically oxidized glass-like carbon samples, J. Mater. Sci. 35 (2000) 139–146.

[53] Louette P, Bodino F, Pireaux J-J, Poly(ethylene terephthalate) (PET) XPS Reference Core Level and Energy Loss Spectra, Surf. Sci. Spectra. 12 (2005) 1. doi:10.1116/11.20050203.

[54] Nakamura H, Nakamura T, Noguchi T, Imagawa K, Photodegradation of PEEK sheets under tensile stress, Polym. Degrad. Stab. 91 (2006) 740–746. doi:10.1016/j.polymdegradstab.2005.06.003.

[55] Torres D, Pinilla JL, Moliner R, Suelves I, On the oxidation degree of few-layer

graphene oxide sheets obtained from chemically oxidized multiwall carbon nanotubes, Carbon. 81 (2015) 405–417. doi:https://doi.org/10.1016/j.carbon.2014.09.073.

[56] Dimiev AM, Alemany LB, Tour JM, Graphene oxide. Origin of acidity, its instability in water, and a new dynamic structural model, ACS Nano. 7 (2013) 576–588. doi:10.1021/nn3047378.

[57] Paredes JI, Villar-Rodil S, Solís-Fernández P, Martínez-Alonso A, Tascón JMD, Atomic Force and Scanning Tunneling Microscopy Imaging of Graphene Nanosheets Derived from Graphite Oxide, Langmuir. 25 (2009) 5957–5968. doi:10.1021/la804216z.

[58] Chen D, Feng H, Li J, Graphene Oxide: Preparation, Functionalization, and Electrochemical Applications, Chem. Rev. 112 (2012) 6027–6053. doi:10.1021/cr300115g.

[59] Wei B, Xu X, Jin Z, Tian Y, Surface Chemical Compositions and Dispersity of Starch Nanocrystals Formed by Sulfuric and Hydrochloric Acid Hydrolysis, PLoS One. 9 (2014) e86024. doi:10.1371/journal.pone.0086024.

[60] Johansson L-S, Campbell JM, Reproducible XPS on biopolymers: cellulose studies, Surf. Interface Anal. 36 (2004) 1018–1022. doi:10.1002/sia.1827.

[61] Liu H, Jiang Y, Tan W, Wang X, Liu H, Jiang Y, et al., Enhancement of the Laser Transmission Weldability between Polyethylene and Polyoxymethylene by Plasma Surface Treatment, Materials (Basel). 11 (2017) 29. doi:10.3390/ma11010029.

[62] Eigler S, Dotzer C, Hof F, Bauer W, Hirsch A, Sulfur Species in Graphene Oxide,

Chem. – A Eur. J. 19 (2013) 9490–9496. doi:10.1002/chem.201300387.

[63] Radovic LR, Rodriguez-Reinoso F, Carbon Materials in Catalysis, in: P.A. Thrower (Ed.), Chem. Phys. Carbon, Vol. 25, Marcel Dekker, New York, 1995: pp. 243–358.

[64] Szymański GS, Karpiński Z, Biniak S, Świątkowski A, The effect of the gradual thermal decomposition of surface oxygen species on the chemical and catalytic properties of oxidized activated carbon, Carbon. 40 (2002) 2627–2639. doi:10.1016/S0008-6223(02)00188-4.

[65] Fan X, Peng W, Li Y, Li X, Wang S, Zhang G, et al., Deoxygenation of Exfoliated Graphite Oxide under Alkaline Conditions: A Green Route to Graphene Preparation, Adv. Mater. 20 (2008) 4490–4493. doi:10.1002/adma.200801306.

[66] Johra FT, Lee J-W, Jung W-G, Facile and safe graphene preparation on solution based platform, J. Ind. Eng. Chem. 20 (2014) 2883–2887. doi:10.1016/J.JIEC.2013.11.022.

[67] Kang JH, Kim T, Choi J, Park J, Kim YS, Chang MS, et al., Hidden Second Oxidation Step of Hummers Method, Chem. Mater. 28 (2016) 756–764. doi:10.1021/acs.chemmater.5b03700.

[68] Chen X, Chen B, Direct Observation, Molecular Structure, and Location of Oxidation Debris on Graphene Oxide Nanosheets, Environ. Sci. Technol. 50 (2016) 8568–8577. doi:10.1021/acs.est.6b01020.

[69] Lavin-Lopez M del P, Romero A, Garrido J, Sanchez-Silva L, Valverde JL, Influence of Different Improved Hummers Method Modifications on the Characteristics of Graphite Oxide in Order to Make a More Easily Scalable Method,

Ind. Eng. Chem. Res. 55 (2016) 12836–12847. doi:10.1021/acs.iecr.6b03533.

[70] Donelli I, Freddi G, Nierstrasz VA, Taddei P, Surface structure and properties of poly-(ethylene terephthalate) hydrolyzed by alkali and cutinase, Polym. Degrad. Stab. 95 (2010) 1542–1550. doi:10.1016/j.polymdegradstab.2010.06.011.

[71] Pan S, Aksay IA, Factors controlling the size of graphene oxide sheets produced via the graphite oxide route, ACS Nano. 5 (2011) 4073–4083. http://www.scopus.com/inward/record.url?eid=2-s2.0-80051483707&partnerID=40&md5=b13e4aebab5fdd8736f8b9b1c2506cd1.

[72] Wissler M, Graphite and carbon powders for electrochemical applications, J. Power Sources. 156 (2006) 142–150. doi:10.1016/J.JPOWSOUR.2006.02.064.

[73] Shen L, Zhang L, Wang K, Miao L, Lan Q, Jiang K, et al., Analysis of oxidation degree of graphite oxide and chemical structure of corresponding reduced graphite oxide by selecting different-sized original graphite, RSC Adv. 8 (2018) 17209–17217. doi:10.1039/C8RA01486H.

[74] Trömel M, Russ M, Dimanganheptoxid zur selektiven Oxidation organischer Substrate, Angew. Chemie. 99 (1987) 1037–1038. doi:10.1002/ange.19870991009.

[75] Dimiev A, Kosynkin D V., Alemany LB, Chaguine P, Tour JM, Pristine Graphite Oxide, J. Am. Chem. Soc. 134 (2012) 2815–2822. doi:10.1021/ja211531y.

[76] Beckett RJ, Croft RC, The Structure of Graphite Oxide, J. Phys. Chem. 56 (1952) 929–935. doi:10.1021/j150500a001.

[77] Chen J, Li Y, Huang L, Li C, Shi G, High-yield preparation of graphene oxide from small graphite flakes via an improved Hummers method with a simple purification

process, Carbon. 81 (2015) 826–834. doi:10.1016/J.CARBON.2014.10.033.

[78] Eigler S, Enzelberger-Heim M, Grimm S, Hofmann P, Kroener W, Geworski A, et al., Wet Chemical Synthesis of Graphene, Adv. Mater. 25 (2013) 3583–3587. doi:10.1002/adma.201300155.

[79] Wolfe S, Ingold CF, Oxidation of olefins by potassium permanganate. Oxygen-labeling experiments and mechanism of the oxidation of 1,5-hexadiene. Evidence for a manganese intermediate with coordination number greater than four, J. Am. Chem. Soc. 103 (1981) 940–941. doi:10.1021/ja00394a038.

[80] Rajender G, Giri PK, Formation mechanism of graphene quantum dots and their edge state conversion probed by photoluminescence and Raman spectroscopy, J. Mater. Chem. C. 4 (2016) 10852–10865. doi:10.1039/C6TC03469A.

[81] Xing Y, Lu P, Wang J, Yang J, Chen Y, Defect-induced selective oxidation of graphene: A first-principles study, Appl. Surf. Sci. 396 (2017) 243–248. doi:10.1016/J.APSUSC.2016.10.086.

[82] Rangel NL, Sotelo JC, Seminario JM, Mechanism of carbon nanotubes unzipping into graphene ribbons, J. Chem. Phys. 131 (2009) 031105. doi:10.1063/1.3170926.

[83] Silva-Tapia AB, García-Carmona X, Radovic LR, Similarities and differences in O2 chemisorption on graphene nanoribbon vs. carbon nanotube, Carbon. 50 (2012) 1152–1162. doi:10.1016/j.carbon.2011.10.028.

[84] Yang M, Hu L, Tang X, Zhang H, Zhu H, Fan T, et al., Longitudinal splitting versus sequential unzipping of thick-walled carbon nanotubes: Towards controllable synthesis of high-quality graphitic nanoribbons, Carbon. 110 (2016) 480–489.

doi:10.1016/J.CARBON.2016.09.055.

[85] Li J-L, Kudin KN, McAllister MJ, Prud'homme RK, Aksay IA, Car R, Oxygen-Driven Unzipping of Graphitic Materials, Phys. Rev. Lett. 96 (2006) 176101. http://link.aps.org/doi/10.1103/PhysRevLett.96.176101.

[86] Sun T, Fabris S, Mechanisms for Oxidative Unzipping and Cutting of Graphene, Nano Lett. 12 (2012) 17–21. doi:10.1021/nl202656c.

[87] Peng X, Misewich JA, Wong SS, Sfeir MY, Efficient Charge Separation in Multidimensional Nanohybrids, Nano Lett. 11 (2011) 4562–4568. doi:10.1021/nl2016625.

[88] Wijewardena UK, Brown SE, Wang X-Q, Epoxy-Carbonyl Conformation of Graphene Oxides, J. Phys. Chem. C. 120 (2016) 22739–22743. doi:10.1021/acs.jpcc.6b07648.

[89] Liu Z, Nørgaard K, Overgaard MH, Ceccato M, Mackenzie DMA, Stenger N, et al., Direct observation of oxygen configuration on individual graphene oxide sheets, Carbon. 127 (2018) 141–148. doi:10.1016/J.CARBON.2017.10.100.

[90] Li Z, Zhang W, Luo Y, Yang J, Hou JG, How Graphene Is Cut upon Oxidation?, J. Am. Chem. Soc. 131 (2009) 6320–6321. doi:10.1021/ja8094729.

[91] Gao X, Jiang DE, Zhao Y, Nagase S, Zhang S, Chen Z, Theoretical insights into the structures of graphene oxide and its chemical conversions between graphene, J. Comput. Theor. Nanosci. 8 (2011) 2406–2422. http://www.scopus.com/inward/record.url?eid=2-s2.0-84863012295&partnerID=40&md5=4170f2836e9a270f882c26deaeac789b.

[92] Leon-y-Leon C, Radovic LR, Interfacial chemistry and electrochemistry of carbon surfaces, in: P.A. Thrower (Ed.), Chem. Phys. Carbon, Vol. 24, 1994: pp. 213–310.

[93] Boehm HP, Surface oxides on carbon and their analysis: a critical assessment, Carbon. 40 (2002) 145–149. http://www.sciencedirect.com/science/article/B6TWD-44N3C70-3/2/1c26dae3d7f09f012a9fe57066721748.

[94] Figueiredo JL, Pereira MFR, The role of surface chemistry in catalysis with carbons, Catal. Today. 150 (2010) 2–7. doi:10.1016/J.CATTOD.2009.04.010.

[95] Perera D, Abeywickrama A, Zen F, Colavita PE, Jayasundara DR, Evolution of oxygen functionalities in graphene oxide and its impact on structure and exfoliation: An oxidation time based study, Mater. Chem. Phys. 220 (2018) 417–425. doi:10.1016/J.MATCHEMPHYS.2018.08.072.

[96] Wolfe S, Ingold CF, Lemieux RU, Oxidation of olefins by potassium permanganate. Mechanism of α-ketol formation, J. Am. Chem. Soc. 103 (1981) 938–939. http://www.scopus.com/inward/record.url?eid=2-s2.0-0000990582&partnerID=40&md5=685cc1abdf584d0394334b005f967ee2.

[97] Dave SH, Gong C, Robertson AW, Warner JH, Grossman JC, Chemistry and Structure of Graphene Oxide *via* Direct Imaging, ACS Nano. 10 (2016) 7515–7522. doi:10.1021/acsnano.6b02391.

[98] Hatcher PG, VanderHart DL, Earl WL, Use of solid-state 13C NMR in structural studies of humic acids and humin from Holocene sediments, Org. Geochem. 2 (1980) 87–92. doi:10.1016/0146-6380(80)90024-8.

[99] Hatcher PG, Rowan R, Mattingly MA, 1H and 13C NMR of marine humic acids,

Org. Geochem. 2 (1980) 77–85. doi:10.1016/0146-6380(80)90023-6.

Declaration of interests

☒ The authors declare that they have no known competing financial interests or personal relationships that could have appeared to influence the work reported in this paper.

☐The authors declare the following financial interests/personal relationships which may be considered as potential competing interests: